Journal of Applied Fluid Mechanics, Vol. 13, No. 4, pp. 1149-1156, 2020.
Available online at www.jafmonline.net, ISSN 1735-3572, EISSN 1735-3645.
DOI: 10.36884/jafm.13.04.30836

Electroosmotic Flow of Salt-Free Power-Law Fluids in Micro/Nanochannels with Fluid Slip

S. H. Chang

Department of Mechanical Engineering, Far East University, Tainan, 74448, Taiwan

† *Email: shchang@mail.feu.edu.tw*

(Received August 7, 2019; accepted December 8, 2019)

ABSTRACT

Electroosmotic flow of salt-free power-law fluids through planar slit and cylindrical micro and nanochannels with fluid slip is theoretically analyzed. Analytical solutions are obtained to investigate the effects of flow behavior index, channel size, applied electric field strength, Gouy-Chapman length (or surface charge density), and fluid slip length on the velocity distribution and volumetric flow rate. The results show that the electroosmotic flow velocity and thereby the flow rate for shear-thinning fluids are many times larger than those for Newtonian and shear-thickening fluids for the ranges of applied electric field strength and surface charge density usually encountered in practice. Such augmentation can be further amplified by increasing the surface charge density, applied electric field strength and fluid slip. Furthermore, the electroosmotic flow velocity profile of shear-thinning fluids becomes more plug-like as the ratio of channel half-width (or radius) to Gouy-Chapman length increases. However, such a profile for shear-thickening fluids always exhibits a parabolic-like flow pattern regardless of the ratios of channel half-width (or radius) to Gouy-Chapman length.

Keywords: Electroosmotic flow; Power-law fluid; Counterion-only; Fluid slip.

NOMENCLATURE

B	nondimensional slip length
b	slip length
c	Dummy constant
E	applied electric field strength
e	elementary charge
h	half-width or radius of channel
k_b	Boltzmann constant
m	geometry index
n	flow behavior index
Q	volumetric flow rate
R	nondimensional transverse coordinat
R_Q	ratio of total flow rate to the flow rate without fluid slip
r	transverse coordinate
s	Dummy variable
T_a	absolute temperature
u	axial velocity function
z	ionic valence
γ	flow consistency index
ε	dielectric constant of the fluid
ε_0	permittivity of vacuum
λ	Gouy-Chapman length
μ	viscosity of the salt-free power-law fluid
σ_s	surface charge density
ψ	electric potential field

1. INTRODUCTION

Electroosmosis is one of the basic electrokinetic phenomena in which the ionized fluid flows through a stationary charged surface when an external electric field is applied. Owing to its numerous advantages such as ease of fabrication, no moving parts, plug-like velocity profile, high reliability, no noise and better flow control, electroosmotic transport has been widely used in chemical and biomedical analysis (Harrison *et al.* 1993; Manz *et al.* 1994), fuel cells (Eikerling *et al.* 2001), and micro/nanofluidic devices (Laser and Santiago, 2004; Manz *et al.* 1994; Stone *et al.* 2004). Electroosmotic flow (EOF) of Newtonian fluids in micro and nanochannels has been well studied over the years (Burgreen and Nakache, 1964; Levine *et al.* 1975; Mala *et al.* 1997; Rice and Whitehead, 1965; Xuan and Li, 2005; Yan *et al.* 2007, 2009). However, many fluids, which are often analyzed in micro and nano-fluidic systems, such biofluids, polymer solutions and colloidal suspensions, are non-Newtonian in nature. This non-Newtonian effect on EOF was first investigated by Bello *et al.* (1994) who found that the experimentally measured electroosmotic velocity of a polymer (methyl cellulose) solution is much higher than that predicted with the classic Helmholtz-Smoluchowski velocity. About a decade later, Das and Chakraborty (2006) obtained the first analytical solution for EOF of power-law fluids in slit microchannels with Debye-Hückel linear approximation. Since then, many theoretical (Berli and Olivares, 2008; Chang, 2016; Escandón *et al.* 2015; Vasu and De, 2010; Zhao and Yang, 2012; Zhao *et al.* 2008), numerical (Tan *et al.* 2009; Zimmerman *et al.* 2006), and experimental (Berli, 2010; Chang and Tsao, 2007; Olivares *et al.* 2009) studies have been reported on EOF of non-Newtonian fluids in micro and nano-channels. For more details about electroosmosis of non-Newtonian fluids, the reader is referred to the review articles (Zhao and Yang, 2013) and the references therein.

All the aforementioned studies are based on the no-slip boundary condition. However, apparent fluid slip has been observed in recent experiments (Choi *et al.* 2003; Pit *et al.* 2000; Tretheway and Meinhart, 2002) at the micro/nano scales. The conventional silica channel surface used in micro and nano-fluidic devices is hydrophilic, while hydrophobic polymers such as poly (dimethylsiloxane) (PDMS) have become increasingly attractive in fabricating such devices (Duffy *et al.* 1998; Ocbvirk *et al.* 2000). The pioneering research of fluid slip effect on EOF of Newtonian fluids was probably done by Muller *et al.* (1986). Later, several works (Ajdari and Bocquet, 2006; Joly *et al.* 2004; Yang and Kwok, 2003) reported in the literature discussed the role of Newtonian fluid slip in the electrokinetic flow over hydrophobic surfaces. Recently, Misra and Sinha (2015) theoretically investigated the non-Newtonian and slip effects on EOF and heat transfer of a second grade fluid in hydrophobic microchannels. Each of these papers revealed a common feature that fluid slip could considerably enhance EOF velocity, thereby increasing the electroosmotic mobility and flow rate.

The working fluids in the above mentioned studies are limited to the electrolyte solutions containing both co-ions and counterions. However, salt-free solutions in which counterions are only present in the media are common in lamellar liquid crystals formed by ionic amphiphiles (Engström and Wennerström, 1978), and also when, for example, colloidal particles, clay sheets, surfactant micelles or bilayers whose surfaces contain ionizable groups interact in water (Israelachvili, 1991). Recently, the low-permittivity organic solvents used in electronic paper (Chang *et al.* 2010) and the proton-water complexes in polymer electrolyte membranes (Eikerling *et al.* 2001) are also found to be salt-free media. Even an electrolyte solution with low salt concentration (< 10^{-5}M) can be treated as a salt-free solution (van der Heyden *et al.* 2006). An exact solution for EOF of a proton-water solution in a cylindrical nanochannel of polymer electrolyte membranes was presented by Berg and Ladipo (2009). Recent theoretical works for transient EOF of salt-free fluids in microchannels (Chang, 2009, 2010, 2012) have shown that the electroosmotic mobility is dependent on the microchannel size, which is completely different from that in an electrolyte solution. This result has been validated with EOF experiments (Chang *et al.* 2010). More recently, Bandopadhyay and Chakraborty (2013) investigated the effect of ionic size on electroosmotic transport of salt-free solution through nanochannels. Unfortunately, none of these studies address the non-Newtonian or fluid slip effects on EOF of salt-free fluids.

The objective of this paper is to present a theoretical description of the EOF of a salt-free power-law fluid in slit and cylindrical micro/nanochannels with fluid slip. For this purpose, the mathematical formulation of the problem and the resulting analytical expressions of the EOF velocity and volumetric flow rate are given in Section 2. Then, parametric studies are conducted to investigate the effects of flow behavior index, channel size, applied electric field strength, Gouy-Chapman length (or surface charge density), and fluid slip on the EOF velocity distribution and volumetric flow rate in Section 3. Finally, a summary of the main results is provided in Section 4.

2. MATHEMATICAL MODELLING

Consider an infinitely long planar slit of width $2h$ or cylindrical capillary of radius h, uniformly charged with the surface charge density σ_s and filled with a power-law fluid containing only counterions of the valence $-z$, as shown in Fig. 1. Then, for the planar slit ($m=0$), the electric potential field $\psi(r)$ has been derived as (Chang, 2010)

$$\psi(r) = \frac{k_b T_a}{ze} \ln \sec^2\left(\frac{cr}{h}\right) \tag{1}$$

while for the cylindrical capillary ($m=1$) (Chang, 2009)

$$\psi(r) = -\frac{2k_b T_a}{ze} \ln\left[1 - \frac{h}{2\lambda+h}\left(\frac{r}{h}\right)^2\right] \tag{2}$$

where e is the elementary charge, k_b is the Boltzmann constants, T_a is the absolute temperature and the constant c in Eq. (1) can be determined by

$$2c\tan c = \frac{hez\sigma_s}{\varepsilon\varepsilon_0 k_b T_a} = \frac{2h}{\lambda} \tag{3}$$

Here, ε is the dielectric constant of the fluid, ε_0 is the permittivity of the vacuum, and the Gouy-Chapman length

$$\lambda = \frac{2\varepsilon\varepsilon_0 k_b T_a}{ze\sigma_s} \tag{4}$$

defines a layer near the charged surface within which most counterions are localized (van der Heyden *et al.* 2006). Note that λ is inversely proportional to the surface charge density σ_s and play a similar role as the Debye length does in electrolyte solutions.

When a uniform external electric field E is applied along the negative axial direction, the fluid starts to move due to electroosmosis. Also, no pressure gradient is applied and gravitational force is negligible. For an axisymmetric, steady, fully developed flow, only the axial velocity $u(r)$ exists and then the momentum equation can be simplified to

$$\frac{d}{dr}\left(r^m \mu \frac{du}{dr}\right) + E\varepsilon\varepsilon_0 \frac{d}{dr}\left(r^m \frac{d\psi}{dr}\right) = 0 \tag{5}$$

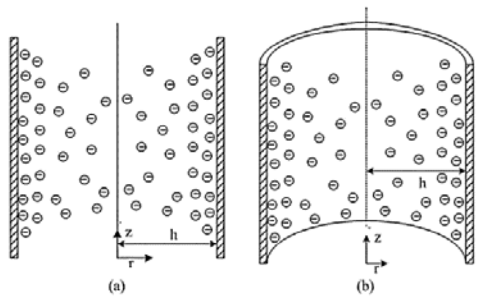

Fig. 1. Schematic diagrams of the symmetrically charged (a) planar slit of width 2h and (b) cylindrical capillary of radius h, filled with a power-law fluid containing only mobile counterions.

where μ is the viscosity of a salt-free power-law fluid and given by (Chhabra and Richardson, 1999)

$$\mu = \gamma\left(-\frac{du}{dr}\right)^{n-1} \tag{6}$$

Here, γ is the flow consistency index and n is the flow behavior index. Note that the power-law fluids are classified as the shear-thinning (pseudoplstic) fluids for n <1, Newtonian fluids for n =1, or the shear-thickening (dilatant) fluids for n >1. Substitute Eq. (6) into Eq. (5) to give

$$\frac{d}{dr}\left[r^m \gamma\left(-\frac{du}{dr}\right)^n\right] - E\varepsilon\varepsilon_0 \frac{d}{dr}\left(r^m \frac{d\psi}{dr}\right) = 0 \tag{7}$$

which is subject to the symmetry at center (r =0) and Navier's slip condition at wall (r = h), i.e.

$$\left.\frac{du}{dr}\right|_{r=0} = 0,\ u(h) = -b\left.\frac{du}{dr}\right|_{r=h} \tag{8}$$

where b is the slip length and positive. Note that the negative sign is chosen in Eqs. (6) and (8) because the velocity decreases with an increase in r in both cases.

The exact solution to Eq. (7) with the boundary conditions Eq. (8) can be derived as

$$u(r) = \int_r^h \left(\frac{E\varepsilon\varepsilon_0}{\gamma}\frac{d\psi}{dr}\right)^{\frac{1}{n}} ds - b\left.\frac{du}{dr}\right|_{r=h} \tag{9}$$

After substituting Eq. (1) into the above equation, we obtain the EOF velocity through the planar slit (m=0)

$$u(r) = h\left(\frac{2E\varepsilon\varepsilon_0 k_b T_a}{\gamma z e \lambda}\right)^{\frac{1}{n}}\left\{\int_R^1\left[\frac{\tan(cs)}{\tan c}\right]^{\frac{1}{n}} ds + B\right\} = h\left(\frac{E\sigma_s}{\gamma}\right)^{\frac{1}{n}}\left\{\int_R^1\left[\frac{\tan(cs)}{\tan c}\right]^{\frac{1}{n}} ds + B\right\} \tag{10}$$

where R = r/h and B =b/h. Furthermore, the volumetric flow rate per unit length of the planar slit channel can be expressed as

$$Q = 2h^2\left(\frac{E\sigma_s}{\gamma}\right)^{\frac{1}{n}}\left\{\int_0^1\int_R^1\left[\frac{\tan(cs)}{\tan c}\right]^{\frac{1}{n}} ds\,dR + B\right\} \tag{11}$$

where the first term represents the flow rate without fluid slip (i.e. B =0) and the ratio of total flow rate to this flow rate becomes

$$R_Q = 1 + \frac{B}{\int_0^1\int_R^1\left[\frac{\tan(cs)}{\tan c}\right]^{\frac{1}{n}} ds\,dR} \tag{12}$$

Similarly, the EOF velocity in a cylindrical capillary (m =1) can be obtained from Eqs. (2) and (9) as

$$u(r) = h\left(\frac{2E\varepsilon\varepsilon_0 k_b T_a}{\gamma z e \lambda}\right)^{\frac{1}{n}}\left\{\int_R^1\left[\frac{2s}{2+\frac{h}{\lambda}\left(1-s^2\right)}\right]^{\frac{1}{n}} ds + B\right\} = h\left(\frac{E\sigma_s}{\gamma}\right)^{\frac{1}{n}}\left\{\int_R^1\left[\frac{2s}{2+\frac{h}{\lambda}\left(1-s^2\right)}\right]^{\frac{1}{n}} ds + B\right\} \tag{13}$$

and the volumetric flow rate is

$$Q = 2\pi h^3\left(\frac{E\sigma_s}{\gamma}\right)^{\frac{1}{n}}\left\{\int_0^1\int_R^1\left[\frac{2s}{2+\frac{h}{\lambda}(1-s^2)}\right]^{\frac{1}{n}} ds\,R\,dR + \frac{B}{2}\right\} \tag{14}$$

with corresponding ratio of the total flow rate to the flow rate without fluid slip

$$R_Q = 1 + \frac{B}{2\int_0^1\int_R^1\left[\frac{2s}{2+\frac{h}{\lambda}(1-s^2)}\right]^{\frac{1}{n}} ds\,R\,dR} \tag{15}$$

It is apparent from the above equations that the fluid slip B can enhance the EOF velocity and thereby the flow rate. Also, the EOF velocity and the flow rate are nonlinear with both parameters h/λ and $E\sigma_s/\gamma$ due to the non-Newtonian fluid behavior. Moreover, the ratio of volumetric flow rate with fluid slip to that without fluid slip depends only on n, B, and h/λ, not on $E\sigma_s/\gamma$.

3. RESULTS AND DISCUSSION

The working fluid is assumed to be a power-law fluid containing only monovalent counterions (z=1). Other parameters used in calculations are dielectric constant of medium ε=24.3 for ethanol (Chang *et al.* 2010), room temperature T_a=298 K, and flow consistency index γ=10^{-2} Pa s^n (Berli and Olivares, 2008). Hence, it follows from Eq. (4) that the relation between the surface charge density σs and the Gouy-Chapman length λ becomes $\lambda\ \sigma_s \fallingdotseq 1.105 \times 10^{-11}$ Cm^{-1}. This implies that σ_s=10^{-2} Cm^{-2} yields λ≒1.1 nm. A direct numerical integration was applied to compute the EOF velocity and the flow rate using quad8.m in MATLAB and Simpson's rule with 500 grids.

Figure 2 shows the shape of the EOF velocity normalized with its velocity at the centerline of channels $u(0)$ for various salt-free power-law fluids through a planar slit channel without fluid slip at two different ratios of channel half-width (or radius) h to Gouy-Chapman length λ. The corresponding results in a cylindrical capillary without fluid slip are shown in Fig. 3. For shear-thickening fluids (n>1), the velocity profile always exhibits a parabolic-like flow

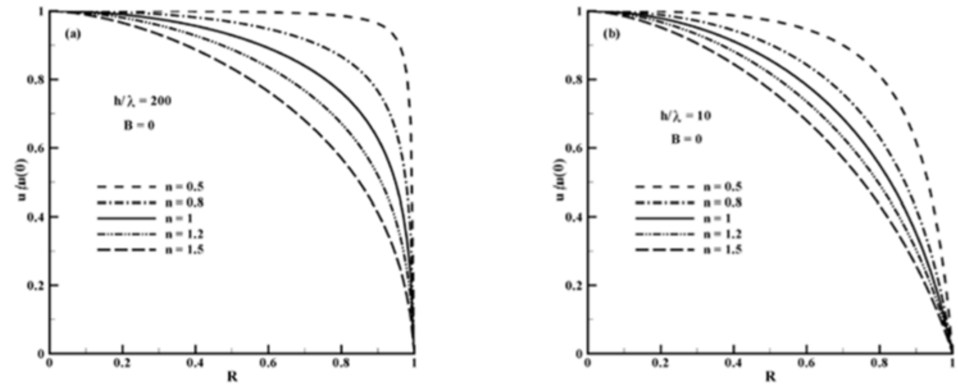

Fig. 2. Spatial profile of the normalized EOF velocity for various salt-free power-law fluids through a planar slit without fluid slip at (a) *h/λ* = 200 and (b) *h/λ* = 10. The reference velocity *u(0)* is the EOF velocity at the centerline of channels.

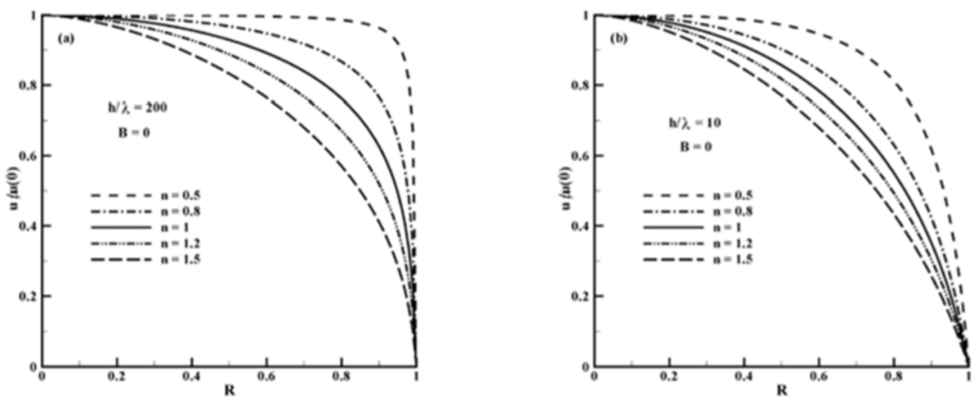

Fig. 3. Spatial profile of the normalized EOF velocity for various salt-free power-law fluids through a cylindrical capillary without fluid slip at (a) *h/λ* = 200 and (b) *h/λ* = 10. The reference velocity *u(0)* is the EOF velocity at the centerline of channels.

pattern regardless of the values of h/λ. For shear-thinning fluids ($n<1$), however, such a profile becomes more plug-like as h/λ increases. This is because the viscosity of shear-thinning fluids decreases significantly near the channel wall with increasing the value of h/λ. It should be pointed out that the fluid slip B and the parameter $E\sigma_s/\gamma$ have no effect on the EOF velocity profile as can be seen from Eqs. (10) and (13).

Figure 4 shows the EOF velocity distributions of various salt-free power-law fluids inside the planar slit channels and cylindrical capillaries without fluid slip for different combinations of the parameters h/λ and $E\sigma_s/\gamma$ while keeping $h=50$ μm. It is clearly seen that the EOF velocity in both geometries increases as $E\sigma_s/\gamma$ increases or h/λ decreases. Also, the EOF velocity in a planar slit channel is always larger than that in a cylindrical capillary provided that the capillary diameter equals to the planar slit width. Nevertheless, such a difference tends to disappear with a decrease in h/λ (see Figs. 4(c) and (d)). This is due to the fact that their EOF velocities given by Eqs. (10) and (13) will approach to the same value as $h/\lambda \rightarrow 0$. Another notable result in Fig. 4 is that the velocity is larger (smaller) for pseudoplastic fluids ($n<1$) than that for dilatant fluids ($n>1$) when $E\sigma_s/\gamma$ is greater (less) than some critical value. Besides, the above critical value of $E\sigma_s/\gamma$ will reach 1 as $h/\lambda \rightarrow 0$ and increase with increasing h/λ. These interesting features stem from the competition between two opposite effects: As the flow behavior index n is raised, the term $(E\sigma_s/\gamma)^{1/n}$ in Eqs. (10) and (13) increases for $E\sigma_s/\gamma <1$ but decreases for $E\sigma_s/\gamma >1$, while the integral appearing in the same equations increases for all values of h/λ. As a result, at higher values of $E\sigma_s/\gamma$, which is enough to counterbalance the effect by a given value of h/λ, an increase in flow behavior index n leads to a reduction in the EOF velocity; however, the opposite is true at low $E\sigma_s/\gamma$.

Since the general behavior of the EOF velocity in both geometries is similar, for brevity, only the results of volumetric flow rates through the cylindrical capillary are presented below. The variation of normalized volumetric flow rate in the cylindrical capillary as a function of the flow behavior index n for various values of $E\sigma_s/\gamma$ while

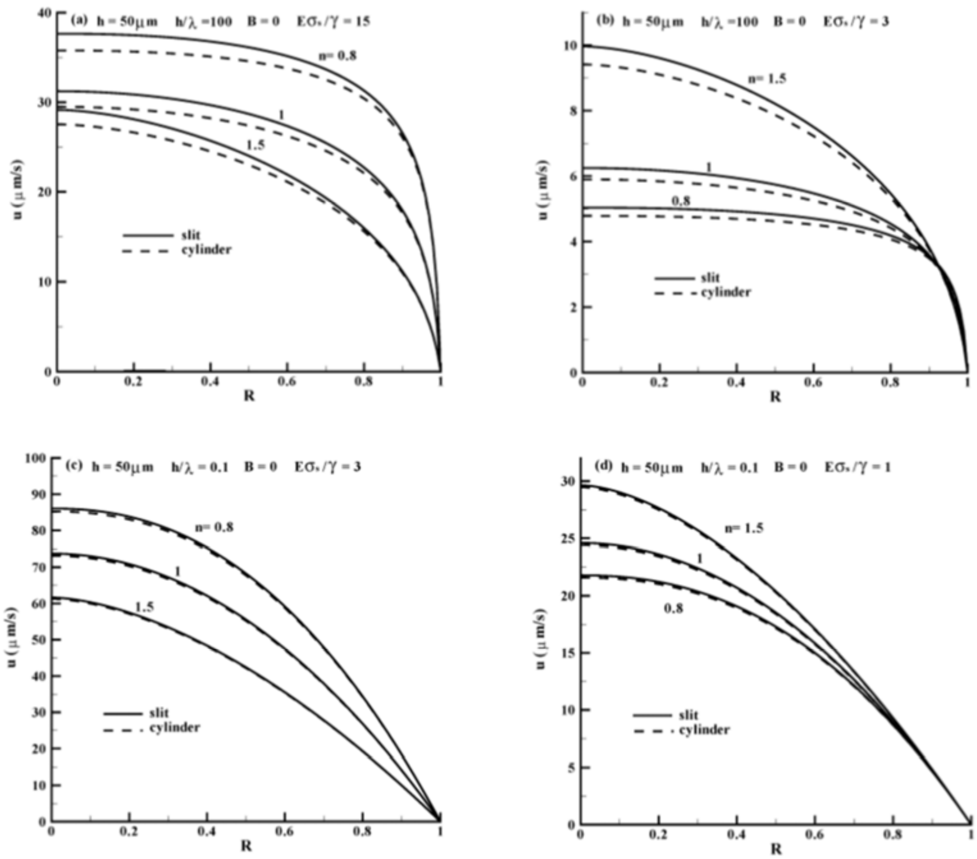

Fig. 4. Spatial distribution of EOF velocity for various salt-free power-law fluids through planar slit (solid lines) and cylindrical (dashed lines) micro/nanochannels without fluid slip at (a) *h/λ* =100, *Eσs/γ* =15s^{-n} (b) *h/λ* =100, *Eσs/γ* =3s^{-n} (c) *h/λ* =0.1, *Eσs/γ* =3s^{-n} and (d) *h/λ* =0.1, *Eσs/γ* =1s^{-n} with a fixed channel half-width (radius) *h* =50μm.

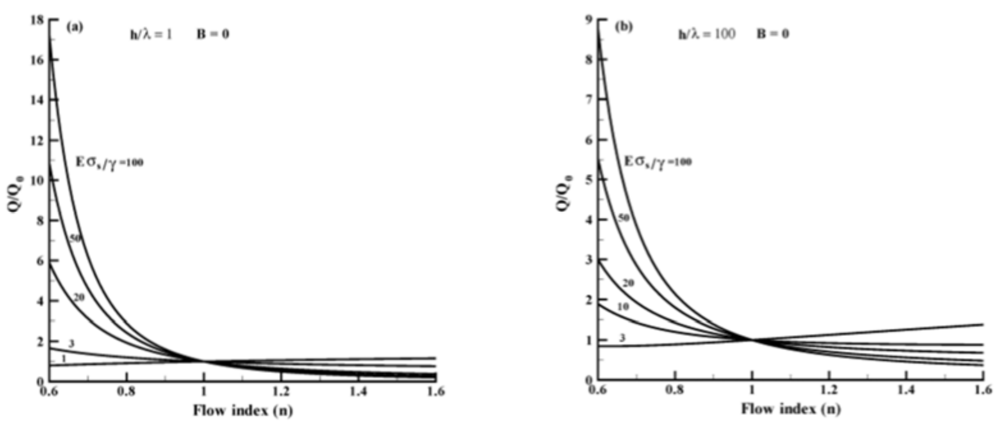

Fig. 5. Variation of the normalized volumetric flow rate for various salt-free power-law fluids through a cylindrical capillary without fluid slip at different values of *Eσs/γ* with(a) *h/λ* = 1 and (b) *h/λ* = 100. The reference flow rate Q_0 is the flow rate of Newtonian fluids (*n =1*) without fluid slip (*B=0*).

keeping h/λ=1 and 100 is displayed in Figs. 5(a) and (b), respectively, without fluid slip ($B=0$). The reference flow rate Q_0 is that of Newtonian fluids ($n=1$) without fluid slip ($B=0$). At higher $E\sigma_s/\gamma$, which is common in practice, the flow rate is expected to decrease rapidly with the flow behavior index at low n ($n<1$) and then tend to remain more or less unchanged at higher n ($n \geq 1$). Under this condition, the volumetric flow rate of shear-thinning fluids ($n<1$) is several times that of Newtonian and

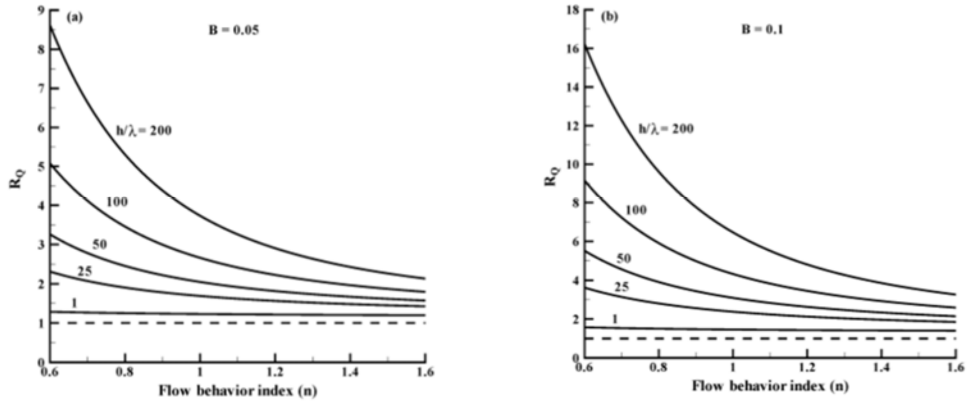

Fig. 6. Ratio R_Q of the flow rate with fluid slip (a) *B* =0.05 and (b) *B* =0.1 to that without fluid slip (*B* =0) in a cylindrical capillary as a function of the flow behavior index *n* for various values of *h/λ*. The dashed line R_Q =1 represents the case without fluid slip (*B* =*0*).

shear-thickening fluids ($n \geq 1$). This enhancement can be greatly enlarged by increasing the value of $E\sigma_s/\gamma$. Similar results have been reported in electrolyte power-law fluids by Zhao *et al*. (2008) and by Vasu and De (2010). At lower $E\sigma_s/\gamma$, the flow rate increases as n increases; however, such an increase is limited. Unlike the shear-thinning fluids, it is practically difficult to increase the volumetric flow rate of shear-thickening fluids. This implies that the shear-thinning fluid is more suitable to be the working fluid than the shear-thickening fluid in electroosmotic pumping.

Figure 6 shows the ratio R_Q of the flow rate with fluid slip (B=0.05 and 0.1) to that without fluid slip ($B=0$) in a cylindrical capillary as a function of the flow behavior index n for various values of h/λ. For a comparison, the result $R_Q= 1$ for the case with $B=0$ is plotted as the dashed line in the figure. As expected, the flow rate is enhanced by increasing the fluid slip, where the largest enhancements are obtained in the region of small n values in which the fluids exhibit the shear-thinning behavior. Such augmentation can be amplified up to about 9 (16) times with a 5 (10) % fluid slip and even more when h/λ >200. Note that a 5% fluid slip (B=0.05) is easily achieved since a fluid slip of B=0.07 (Tretheway and Meinhart, 2002) has been experimentally measured in octadecyltrichlorosilane (OTS) coated microchannels.

4. CONCLUSIONS

A theoretical study on the electroosmotic flow of a salt-free power-law fluid through the planar slit and cylindrical micro/nanochannels with fluid slip has been presented in this paper. The exact analytical solutions for the EOF velocity are obtained by solving nonlinear Poisson-Boltzmann equation and Cauchy momentum equation. Based on the closed-form solutions, the effects of flow behavior index, channel size, applied electric field strength, Gouy-Chapman length (or surface charge density), and fluid slip on the velocity distribution and volumetric flow rate are discussed. The results show that the EOF velocity profile of shear-thinning fluids (n<1) becomes more plug-like as the ratio of channel half-width (or radius) to Gouy-Chapman length increases. However, such a profile for shear-thickening fluids (n>1) always exhibits a parabolic-like flow pattern regardless of the ratios of channel half-width (or radius) to Gouy-Chapman length. Furthermore, the EOF velocity and thereby the flow rate for shear-thinning fluids are many times larger than those for Newtonian and shear-thickening fluids for the ranges of applied electric field strength and surface charge density usually encountered in practice. Such augmentation can be further amplified by increasing the applied electric field strength, surface charge density and fluid slip.

ACKNOWLEDGEMENTS

This work was supported by the Ministry of Science and Technology, Taiwan, R.O.C under Grant No. MOST 104-2221-E-269 -008 and MOST 105-2221-E-269 -003.

REFERENCES

Ajdari, A. and L. Bocquet (2006). Giant amplification of interfacially driven transport by hydrodynamic slip: Diffusio-osmosis and beyond. *Physical Review Letters* 96, 186102.

Bandopadhyay, A. and S. Chakraborty (2013). Ionic size dependent electroosmosis in ion-selective microchannels and nanochannels. *Electrophoresis* 34, 2193-2198.

Bello, M. S., P. De Besi, R. Rezzonico, P. G. Righetti and E. Casiraghi (1994). Electroosmosis of polymer solutions in fused silica capillaries. *Electrophoresis* 15, 623-626.

Berg, P. and K. Ladipo (2009). Exact solution of an electro-osmotic fllow problem in a cylindrical channel of polymer electrolyte membranes. *Proceedings of the Royal Society A: Mathematical, Physical and Engineering*

Sciences 465, 2663-2679.

Berli, C. L. A. (2010). Output pressure and efficiency of electrokinetic pumping of non-Newtonian fluids. *Microfluidics and Nanofluidics* 8, 197-207.

Berli, C. L. A. and M. L. Olivares (2008). Electrokinetic flow of non-Newtonian fluids in microchannels. *Journal of Colloid and Interface Science* 320, 582-589.

Burgreen, D. and F. R. Nakache (1964). Electrokinetic flow in ultrafine capillary slits. *The Journal of Physical Chemistry* 68, 1084-1091.

Chang, F. M. and H. K. Tsao (2007). Drag reduction in electro-osmosis of polymer solutions. *Applied Physics Letters* 90, 194105.

Chang, F. M. and Y. W. Chang, Y. J. Sheng and H. K. Tsao (2010). Size-dependent electro-osmosis in a microchannel with low-permittivity, salt-free media. *Applied Physics Letters* 97, 164101.

Chang, S. H. (2009). Transient electroosmotic flow in cylindrical microcapillaries containing salt-free medium. *Biomicrofluidics* 3, 012802.

Chang, S. H. (2010). Electroosmotic flow in slit microchannel containing salt-free solution. European *Journal of Mechanics B/Fluids* 29, 337-341.

Chang, S. H. (2012). Electroosmotic flow in a dissimilarly charged slit microchannel containing salt-free solution. *European Journal of Mechanics B/Fluids* 34, 85-90.

Chang, S. H. (2016). Comments on “Transient electroosmotic flow of Maxwell fluids with asymmetric zeta potentials through slit microchannel” [Eur. J. Mech. B Fluids 53 (2015) 180–189]. *European Journal of Mechanics B/Fluids* 58, 95-97.

Chhabra, R. P. and J. F. Richardson (1999). *Non-Newtonian Flow in Process Industries: Fundamentals and Engineering Applications*. Butterworth-Heinemann, Oxford.

Choi, C. H., K. J. A. Westin and K. S. Breuer (2003). Apparent slip flows in hydrophilic and hydrophobic microchannels. *Physics of Fluids* 15, 2897–2902.

Das, S. and S. Chakraborty (2006). Analytical solutions for velocity, temperature and concentration distribution in electroosmotic microchannel flows of a non-Newtonian bio-fluid. *Analytica Chimica Acta* 559, 15-24.

Duffy, D. C., J. C. Mcdonald, O. J. A. Schueller and G. M. Whitesides (1998). Rapid prototyping of microfluidic systems in poly (dimethylsiloxane). *Analytical Chemistry* 70, 4974-4984.

Eikerling, M., A. A. Kornyshev, A. M. Kuznetsov, J. Ulstrup and S. Walbran (2001). Mechanisms of proton conductance in polymer electrolyte membranes. *The Journal of Physical Chemistry B* 105, 3646-3662.

Engström, S. and H. Wennerström (1978). Ioncondensation on planar surfaces. A solution of the Poisson-Boltzmann equation for two parallel charged plates. *The Journal of Physical Chemistry* 82, 2711-2714.

Escandón, J., E. Jiménez, C. Hernández, O., Bautista and F. Méndez (2015). Transient electroosmotic flow of Maxwell fluids with asymmetric zeta potentials through slit microchannel. *European Journal of Mechanics B/Fluids* 53, 180-189.

Harrison, D. J., K. Fluri, K. Seiler, Z. H. Fan, C. S. Effenhauser and A. Manz (1993). Micromachining a miniaturized capillary electrophoresis-based chemical analysis system on a chip. *Science* 261, 895-897.

Israelachvili, J. N. (1991). *Intermolecular and Surface Forces*. Academic Press, San Diego, CA.

Joly, L., C. Ybert, E. Trizac and L. Bocquet (2004). Hydrodynamics within the electric double layer on slipping surfaces. *Physical Review Letters* 93,257805.

Laser, D. J. and J. G. Santiago (2004). A review of micropumps. *Journal of Micromechanics and Microengineering* 14, R35-R64.

Levine, S., J. R. Marriott, G. Neale and N. Epstein (1975). Theory of electrokinetic flow in fine cylindrical capillaries at high zeta potential. *Journal of Colloid and Interface Science* 52, 136-149.

Mala, G. M., D. Li and J. D. Dale (1997). Heat transfer and fluid flow in microchannels. *International Journal of Heat and Mass Transfer* 40, 3079-3088.

Manz, A., C. S. Effenhauser, N. Burggraf, D. J. Harrison, K. Seiler and K. Fluri (1994). Electroosmotic pumping and electrophoretic separations for miniaturized chemical analysis system. *Journal of Micromechanics and Microengineering* 4, 257-265.

Misra, J. C. and A. Sinha (2015). Electro-osmotic flow and heat transfer of a non-Newtonian fluid in a hydrophobic microchannel with Navier slip. *Journal of Hydrodynamics* 27, 647-657.

Muller, V. M., I. P. Sergeeva, V. D. Sobolev and N. V. Churaev (1986). Boundary effects in the theory of electrokinetic phenomena. *Colloid Journal of the USSR* 48, 606-614.

Ocbvirk, G., M. Munroe, T. Tang, R. Oleschuk, K. Westra and D. J. Harrison (2000). Electrokinetic control of fluid flow in native poly (dimethylsiloxane) capillary electrophoresis devices. *Electrophoresis* 21, 107-115.

Olivares, M. L., L. Vera-Candioti and C. L. A. Berli (2009). The EOF of polymer solutions. *Electrophoresis* 30, 921-929.

Pit, R., H. Hervet and L. Léger (2000). Direct experimental evidence of slip in hexadecane: Solid interfaces. *Physical Review Letters* 85, 980-983.

Rice, C. L. and R. Whitehead (1965). Electrokinetic flow in narrow cylindrical capillary. *The Journal of Physical Chemistry* 69, 4017-4024.

Stone, H. A., A. D. Stroock and A. Ajdari (2004). Engineering flows in small devices: Microfluidics toward a lab-on-a-chip. *Annual Review of Fluid Mechanics* 36, 381-411.

Tan, G. H., X. F. Li, Y. L. He and W. Q. Tao (2009). Electroosmotic flow of non-Newtonian fluids in microchannels. *Journal of Non-Newtonian Fluid Mechanics* 157, 133-137.

Tretheway, D. C. and C. D. Meinhart (2002). Apparent fluid slip at hydrophobic microchannel walls. *Physics of Fluids* 14, L9-L12.

van der Heyden, F. H. J., D. J. Bonthuis, D. Stein, C. Meyer and C. Dekker (2006). Electrokinetic energy conversion efficiency in nanofluidic channels. *Nano Letters* 6, 2232-2237.

Vasu, N. and S. De (2010). Electroosmotic flow of power-law fluids at high zeta potentials. *Colloids and Surfaces A: Physicochemical and Engineering Aspects* 368, 44-52.

Xuan, X. and D. Li (2005). Electroosmotic flow in microchannels with arbitrary geometry and arbitrary distribution of wall charge. *Journal of Colloid and Interface Science* 289, 291-303.

Yan, D. G., C. Yang and X. Y. Huang (2007). Effect of finite reservoir size on electroosmotic flow in microchannels. *Microfluidics and Nanofluidics* 3, 333-340.

Yan, D. G., C. Yang, L. M. Miao, Y. C. Lam and X. Y. Huang (2009). Enhancement of electrokinetically driven microfluidic T-mixer using frequency modulated electric field and channel geometry effects. *Electrophoresis* 30, 3144-3152.

Yang, J. and D. Y. Kwok (2003). Effect of liquid slip in electrokinetic parallel-plate microchannel flow. *Journal of Colloid and Interface Science* 260, 225-233.

Zhao, C. and C. Yang (2012). Electroosmotic flows of non-Newtonian power-law fluids in a cylindrical microchannel. *Electrophoresis* 34, 662-667.

Zhao, C. and C. Yang (2013). Electrokinetics of non-Newtonian fluids: A review. *Advances in Colloid and Interface Science* 201-202, 94-108.

Zhao, C., E. Zholkovskij, J. H. Masliyah and C. Yang (2008). Analysis of electroosmotic flow of power-law fluids in a slit microchannel. *Journal of Colloid and Interface Science* 326, 503-510.

Zimmerman, W. B., J. M. Rees and T. J. Craven (2006). Rheometry of non-Newtonian electrokinetic flow in a microchannel T-junction. *Microfluidics and Nanofluidics* 2, 481-492.